Limits to Thermal-Piezoresistive Cooling in Silicon Micromechanical Resonators

James M. L. Miller, Haoshen Zhu, *Member, IEEE*, Subramanian Sundaram, Gabrielle D. Vukasin, Yunhan Chen, Ian B. Flader, Dongsuk D. Shin, and Thomas W. Kenny, *Senior Member, IEEE*

***Abstract*— We study thermal-piezoresistive cooling in silicon micromechanical resonators at large currents and high temperatures. Crossing a thermal transition region corresponds to a steep reduction in resonance frequency, an abrupt plateauing in the effective quality factor, and a large increase in thermomechanical fluctuations. Comparing measurements with simulations suggests that the second-order temperature coefficients of elasticity of doped silicon are not sufficient to capture the drop in resonance frequency at large currents. Overall, our results show that there are clear thermal limits to cooling a resonant mode using current-controlled thermal-piezoresistive feedback in silicon. [2020-0205]**

***Index Terms*— MEMS, microresonators, thermal-piezoresistive pumping, thermal conductivity, elastic modulus.**

I. Introduction

MICRO- and nano-electromechanical (MEM/NEM) resonators have wide utility as resonant sensors [1], [2], oscillators [3], and filters [4]. The quality factor (Q), or inverse damping of a resonator, is perhaps the most important property of these systems since it determines the dynamic response and thermomechanical signal-to-noise ratio (SNR). A wide range of phenomena are under investigation for tuning the effective quality factor (Q_{eff}) and inducing oscillations in micro- and and nano-scale resonators [5]–[12]. Feedback-based schemes can suppress Q_{eff}, improving the resonator bandwidth [13]–[16], or enhance Q_{eff} to the onset of self-sustained oscillations. One such mechanism utilizes the thermal-piezoresistive effect, whereby flowing a direct current through thermal actuator beams connected to the vibrating geometry exerts feedback on the mode via the actuator piezoresistance and thermal expansion coefficient [17]–[19]. Compared to the other feedback mechanisms in MEM/NEM resonators, the thermal-piezoresistive effect is distinguished by its ease of implementation; flowing a simple direct current through an appropriately designed resonator can enhance or suppress Q_{eff}, relying on a thermo-electro-mechanical feedback mechanism intrinsic to the device. If a direct current flows through actuators with a negative longitudinal piezoresistive coefficient, the thermal-piezoresistive effect amplifies the vibrations and increases Q_{eff}. Thermal-piezoresistive Q_{eff} enhancement is finding applications in oscillators for e.g. mass-sensing [20]–[23], tuning resonator nonlinearities [24], pre-amplifying signals in resonant sensors [25], [26], and nanoscale radio-frequency amplifiers [27], [28]. Work is ongoing to increase the operating frequency [29], [30], reduce the power consumption [31], and increase the frequency stability [32] of thermal-piezoresistive oscillators and sensors.

If the sign of the thermal-piezoresistive effect is reversed, the feedback acts to suppress the effective quality factor. The sign change can be achieved by utilizing current control in a p-type doped resonator [19], or tuning the lumped electrical parameters in the biasing circuit [17], [33]. The reversed feedback suppresses the thermal fluctuations of the mode, effectively cooling it. Thermal-piezoresistive cooling offers a scheme for simple real-time adjustments in resonant sensor bandwidth [34]. This technique has potential for temporarily and reversibly switching resonant sensors and oscillators into a "safe" mode in preparation for high acceleration shocks, whereby an integrated sensor flows a direct current through the thermal-piezoresistive actuators prior to impact, suppressing Q_{eff} to a fraction of the intrinsic Q, thus mitigating the risk for pull-in associated with high Q structures [35], [36]. An important consideration with thermal-piezoresistive cooling is the limiting behavior at large currents and high temperatures, since these limits must be taken into account during device design to achieve some desired Q_{eff} reduction in practice.

Manuscript received May 16, 2020; revised August 22, 2020; accepted September 2, 2020. Date of publication September 16, 2020; date of current version October 7, 2020. This work was supported in part by the National Science Foundation Collaborative Research Program under award CMMI-1662464. Fabrication was performed in the nano@Stanford labs, which are supported by the National Science Foundation (NSF) as a part of the National Nanotechnology Coordinated Infrastructure under Award ECCS-1542152, with support from the Defense Advanced Research Projects Agency Precise Robust Inertial Guidance for Munitions (PRIGM) Program, managed by Ron Polcawich and Robert Lutwak. The work of James M. L. Miller was supported by the National Defense Science and Engineering Graduate (NDSEG) Fellowship and in part by the E.K. Potter Stanford Graduate Fellowship. The work of Haoshen Zhu was supported in part by the National Natural Science Foundation of China (NSFC) under Grant 61901177, in part by the Fundamental Research Funds for the Central Universities under Grant 2018MS17, and in part by the Guangdong Innovative and Entrepreneurial Research Team Program under Grant 2017ZT07X032. Subject Editor M. Rais-Zadeh. *(Corresponding authors: James M. L. Miller; Haoshen Zhu.)*

James M. L. Miller, Gabrielle D. Vukasin, Yunhan Chen, Ian B. Flader, Dongsuk D. Shin, and Thomas W. Kenny are with the Departments of Mechanical and Electrical Engineering, Stanford University, Stanford, CA 94305 USA (e-mail: jmlm@stanford.edu).

Haoshen Zhu is with the School of Electronics and Information Engineering, South China University of Technology, Guangzhou 510641, China.(e-mail: zhuhs@scut.edu.cn).

Subramanian Sundaram is with the Biological Design Center, Boston University, Boston, MA 02215 USA, and also with the Wyss Institute for Biologically Inspired Engineering, Harvard University, Boston, MA 02115 USA.

Color versions of one or more of the figures in this article are available online at http://ieeexplore.ieee.org.

Digital Object Identifier 10.1109/JMEMS.2020.3022050

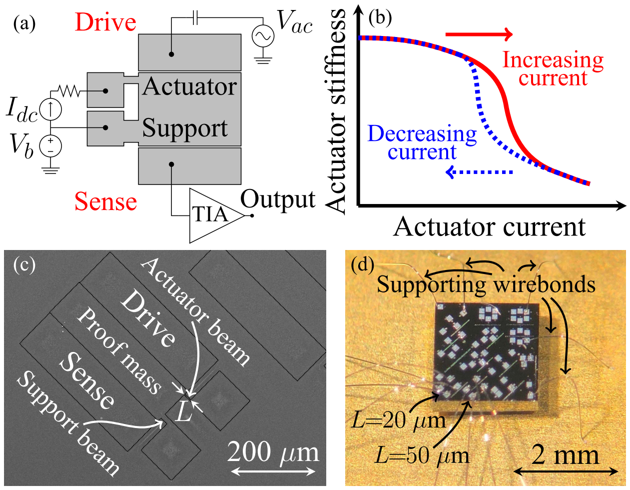

Fig. 1. (a) The measurement setup for the thermal-piezoresistive resonators. Both anchors of the device are voltage-biased at $V_b = 60$ V for capacitive transduction, and a direct current I_{dc} additionally flows through the structure, raising the voltage of the actuator beam anchor with respect to the support beam anchor. The resonator is driven near resonance with $V_{ac} \approx 1$ mV and sensed using a transimpedance amplifier (TIA) connected to the opposing anchor. A 500 Ω resistor is connected in-series with the output of the current source. (b) A depiction of the large current behavior in the actuator of a thermal-piezoresistive resonator. (c) A scanning electron microscope (SEM) image of the device layer of a fabricated thermal-piezoresistive resonator prior to encapsulation. (d) A chip "floated" above the substrate with wirebonds.

This work explores the limiting thermal behavior of thermal-piezoresistive cooling at high temperatures, highlighting the importance of boundary conditions in practice. At large currents, the Joule heating in the resonator results in substantial device heating, with the heating and corresponding temperature rise concentrated in one or more narrow actuator beams where the electrical and thermal resistance is highest. At the large currents typical of the thermal-piezoresistive effect, the current density through the thermal actuator can approach [37], [38] or exceed [39], [40] the $\approx$1 GA/m^2 breakdown current density in silicon, and the properties in the thermal actuator govern the device behavior. The elastic moduli of silicon decrease with temperature, which results in a reducing actuator stiffness with current [41]–[43]. In both n-type-doped and p-type-doped silicon, the electrical conductivity and thermal conductivity both decrease substantially with temperature [44], [45]. These three effects feed on each other at large currents to substantially reduce the extensional stiffness of the thermal actuator, as depicted in Fig. 1(b), thus resulting in a highly nonlinear temperature dependence of resonance frequency. Thermal-piezoresistive resonators exhibit several interesting effects at these large currents.

II. Method and Results

We investigate the limits to thermal-piezoresistive cooling in the cantilevered thermal-piezoresistive resonators depicted in Fig. 1(a, c). The devices are fabricated in a wafer-scale encapsulation process, which produces stable silicon microresonators in an ultra-clean vacuum environment [46], [47]. A fabricated device is shown before and after encapsulation in Figs. 1(c) and 1(d), respectively. The high temperature annealing step inherent to this fabrication process makes our devices well-suited for studying large current effects. We study p-type, moderately boron doped ($N_a \approx 3.4 \times 10^{18}$ cm^{-3}) resonators, with the actuator beam aligned with the $\langle 100 \rangle$-direction. The relatively large electrical resistivity corresponds to a large Joule heating, while the longitudinal piezoresistive coefficient in the $\langle 100 \rangle$ direction is low so the thermal-piezoresistive feedback is relatively weak compared to devices fabricated in the $\langle 110 \rangle$ direction [48]. We previously experimentally and theoretically characterized the low-current thermal-piezoresistive behavior for thermally-grounded devices with a variety of other dopings and orientations [19]. The devices in this study are thermally "floated" above the bond pads with 50 μm diameter wire-bond wires [49], as depicted in Fig. 1(d), which increases the thermal resistance to the ambient temperature, thus enabling a larger temperature rise in the thermal actuators for a given current. Using thermally-floated devices with relatively weak thermal-piezoresistive feedback enables us to access the limiting thermal behavior. The device layer thickness is 40 μm, and the proof mass has a length and width of 360 μm and 100 μm, respectively. The proof mass is supported by a 12 μm wide support beam and a 3 μm wide actuator beam. We measure the fundamental in-plane cantilever mode of the "long-beam" devices with an actuator/support beam length of 50 μm and "short-beam" devices with a 20 μm actuator/support beam length. We use the ring-down technique to extract the Q_{eff} and angular resonance frequency, ω_0, as a function of direct current, since this approach can quickly and accurately obtain the resonator dynamical properties [50]. At each direct current value, a harmonic drive is applied near the resonance frequency, and then shut off while monitoring the vibrations. An exponential function is fit to the decaying amplitude response for each direct current to extract Q_{eff}, and a Fast Fourier Transform (FFT) is utilized to extract ω_0 from the decaying vibrations.

Figure 2 presents the measured effective quality factor and resonance frequency versus direct current, I_{dc}, in devices with an actuator/support beam length of 50 μm and 20 μm. In both devices, the resonance frequency and effective quality factor decrease with increasing current. In the long-beam device at 30 mA, the resonance frequency drops off precipitously while the Q_{eff} plateaus. Increasing the direct current beyond 30 mA results in the slope of the resonance frequency becoming linear with current about a new low frequency state. The behavior in the short beam device is similar, but the current at which the frequency drops off increases to 45 mA.

The abrupt drop in resonance frequency and plateauing in Q_{eff} at large direct current corresponds to a thermal transition in the resonators. We confirm that the transition is a thermal phenomenon with hysteresis measurements and direct thermal infrared (IR) imaging of the chip. For the hysteresis measurements, we measure the resonance frequency while sweeping from low to high direct current, as well as high to low direct current, without giving the device sufficient time to settle to its steady-state temperature at each current. In the thermal transition region, e.g. at $I_{dc} \approx 30$ mA in Fig. 2(a), the resonance frequency is lower for the downward current sweep

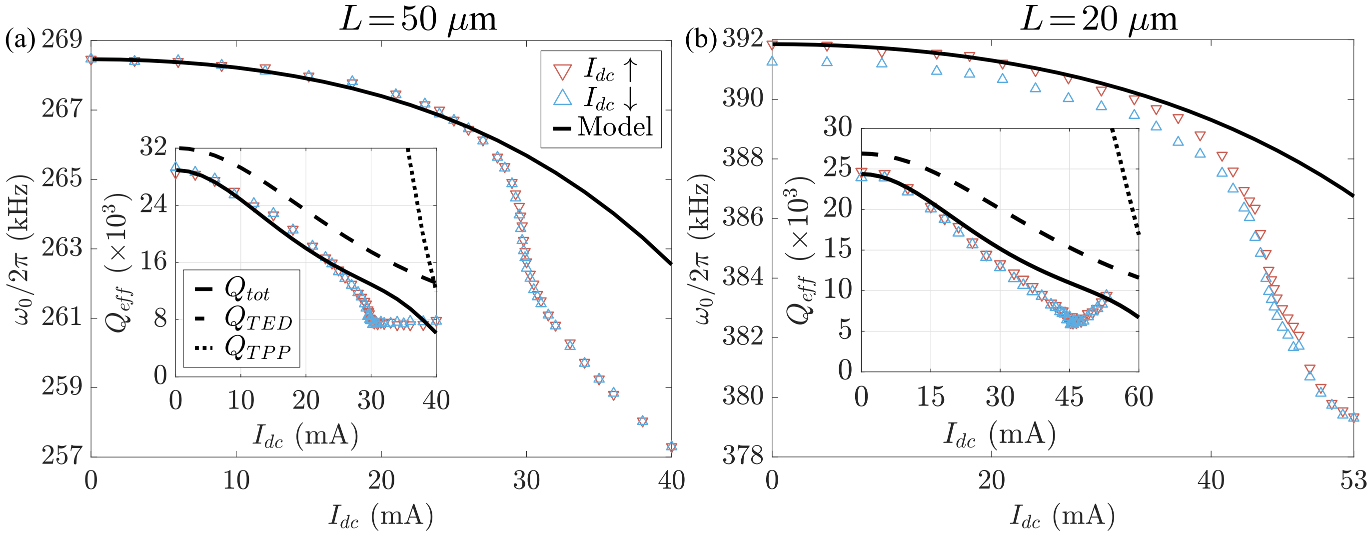

Fig. 2. (a) The measured resonance frequency ($\omega_0/2\pi$) of the 50 μm actuator device for increasing (downward triangles) and decreasing (upward triangles) direct current I_{dc}, with the predicted resonance frequency (solid line). Inset: the corresponding measured and simulated effective quality factor (Q_{eff}), with the simulated contributions from thermoelastic dissipation (Q_{TED}) and thermal-piezoresistive pumping (Q_{TPP}). (b) The same measurements and simulations as in (a), except with the 20 μm actuator device.

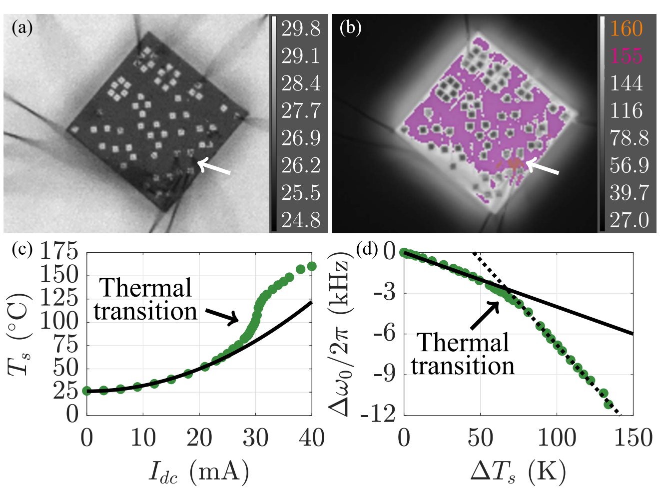

Fig. 3. (a) A thermal infrared (IR) image of the thermally "floated" chip with no direct current in a 25°C ambient environment, with the corresponding temperature scale. The emissivity is calibrated to the top silicon nitride passivation layer (dark gray color) of the chip, and thus the measured temperature for the aluminum bond pads and gold substrate (light gray color) erroneously differ from the ambient temperature. (b) The IR image when 40 mA of direct current flows through the $L = 50\ \mu$m device (white arrow), as in Fig. 2(a). (c) The measured chip surface temperature (T_s) directly above the $L = 50\ \mu$m device as a function of direct current. A quadratic model, $T_s = T_{s,0} + cI_{dc}^2$, for some constant c, is fit to the low current behavior to illustrate the thermal transition. The actual device temperature is much higher than the chip surface temperature. (d) The measured resonance frequency offset $\Delta\omega_0/2\pi = \left[\omega_0(I_{dc}) - \omega_0(0\text{ mA})\right]/2\pi$ versus the change in surface temperature, $\Delta T_s = T_s(I_{dc}) - T_s(0\text{ mA})$, for the measurement in (c). Two linear models are fit to the resonance frequency below and above the thermal transition region.

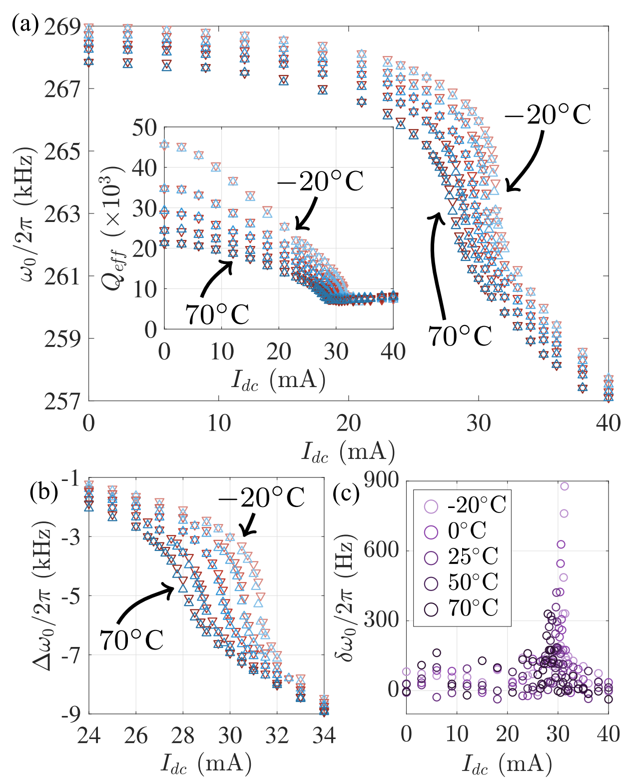

Fig. 4. (a) The measured resonance frequency ($\omega_0/2\pi$) of the $L = 50\ \mu$m device for increasing (downward triangles) and decreasing (upward triangles) direct current I_{dc}, for an ambient temperature of −20°C, 0°C, 25°C, 50°C, and 70°C (light to dark shade). Inset: the corresponding measurements of the effective quality factor (Q_{eff}). (b) The resonance frequency offset $\Delta\omega_0/2\pi = \left[\omega_0(I_{dc}) - \omega_0(0\text{ mA})\right]/2\pi$ versus direct current, in the hysteresis regime. (c) The resonance frequency difference $\delta\omega_0/2\pi = \left[\omega_{0\uparrow}(I_{dc}) - \omega_{0\downarrow}(I_{dc})\right]/2\pi$ between the upward and downward sweep as a function of direct current.

than the upward current sweep. This indicates that the very large shift in resonance frequency in the transition region likely arises from thermal effects. Giving the system sufficient time to equilibrate reduces the frequency hysteresis between the upward and downward current sweeps. The thermal transition region occurs at a larger current for the short-beam device than the long-beam device perhaps because of the lower total electrical and thermal resistance of the shorter actuator beam,

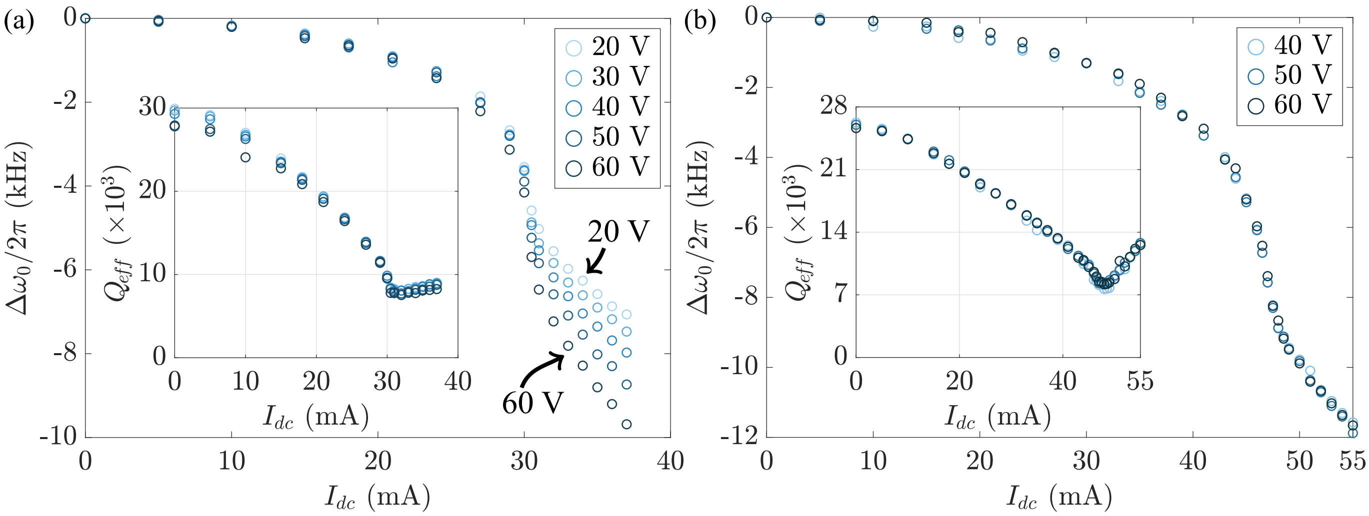

Fig. 5. (a) The measured resonance frequency offset $\Delta\omega_0/2\pi = \left[\omega_0(I_{dc}) - \omega_0(0)\right]/2\pi$ for the 50 μm actuator device as a function of direct current I_{dc}, and different bias voltages, V_b. Inset: the corresponding measured effective quality factor Q_{eff} versus direct current. (b) The same measurements and simulations as in (a), except with the 20 μm actuator device.

which would correspond to a lower actuator temperature for a given direct current.

We employ a FLIR A615 thermal IR camera with a 25 μm resolution lens to image the chip surface temperature as a function of direct current through the long-beam device. These measurements are presented in Fig. 3, and reveal that in the thermal transition region, the chip surface temperature departs from a simple quadratic dependence on direct current. Plotting the shift in resonance frequency for the long-beam device versus measured chip temperature in Fig. 3(d) illustrate two regimes with differing slopes where the change in resonance frequency is proportional to the change in chip surface temperature, demarcated by a thermal transition region.

We develop finite-element (FE) simulations based on COMSOL Multiphysics to model ω_0 and Q_{eff} at various I_{dc} levels in Fig. 2. The FE simulation is divided into two steps. In the first step, a stationary analysis is performed to obtain the elevated temperature profile (T_{dc}) due to Joule heating, as well as the direct current density (J_{dc}). Given that T_{dc} can significantly exceed the anchor temperature at high I_{dc} (over 100 K), the temperature-dependent material properties (i.e. resistivity [45] and thermal conductivity [51]) are used in our model to predict T_{dc}, hence ω_0 and Q_{eff} versus I_{dc}. We additionally compute the deformation of the device induced by thermal expansion at T_{dc}, and treat this as the pre-stressed condition for the subsequent analysis. In the second step, the eigenfrequency analysis is performed to simulate ω_0 as well as the thermoelastic damping (TED) and the thermal-piezoresistive pumping (TPP). Q_{TED} and Q_{TPP} are the two major loss mechanisms for these devices. Based on the simulated T_{dc} and the temperature coefficients of elasticity (TCEs), the ω_0 shift at various I_{dc} values can be obtained. The TCEs up to the second order are adopted from [52]. For the TED simulation, the heat source, thermal conductivity and elastic moduli are set to be T_{dc}-dependent so that the Q_{TED} varies with I_{dc}. For the TPP simulation, we adapt the approach that we reported in [19].

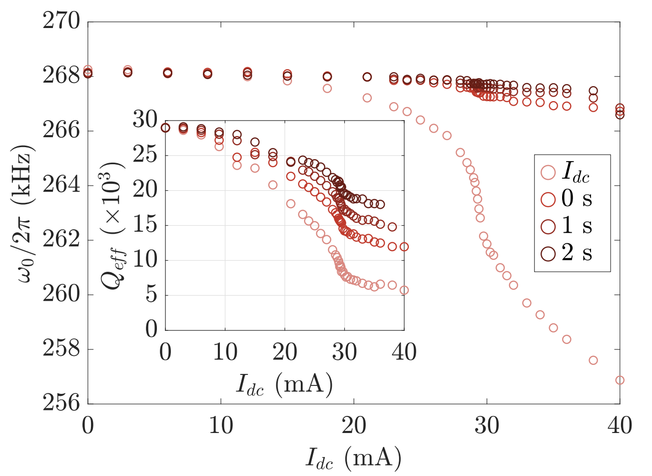

Fig. 6. (a) The measured resonance frequency ($\omega_0/2\pi$) of the $L = 50$ μm device for increasing direct current I_{dc}, with the direct current on (I_{dc}) and off (0 to 3 s) during the ringdown. Inset: the corresponding measurements of the effective quality factor (Q_{eff}).

The predicted resonance frequency and effective quality factor from our model is overlaid on the measurements in Fig. 2. For both devices, the models reproduce the large shift in resonance frequency up to moderate currents, and agree with Q_{eff} up to the thermal transition region. The model does not capture the steep drop in resonance frequency, or the plateauing in Q_{eff} beyond the thermal transition current. We hypothesize that at this point, the actuator material properties become extremely nonlinear, and the TCEs up to second-order and extracted based on a relatively small temperature range (-40 to 85°C) [52] are not sufficient to reproduce the behavior.

The plateauing in the quality factor at the thermal transition region results from the resonator temperature, as opposed to the current density through the actuator. To confirm this,

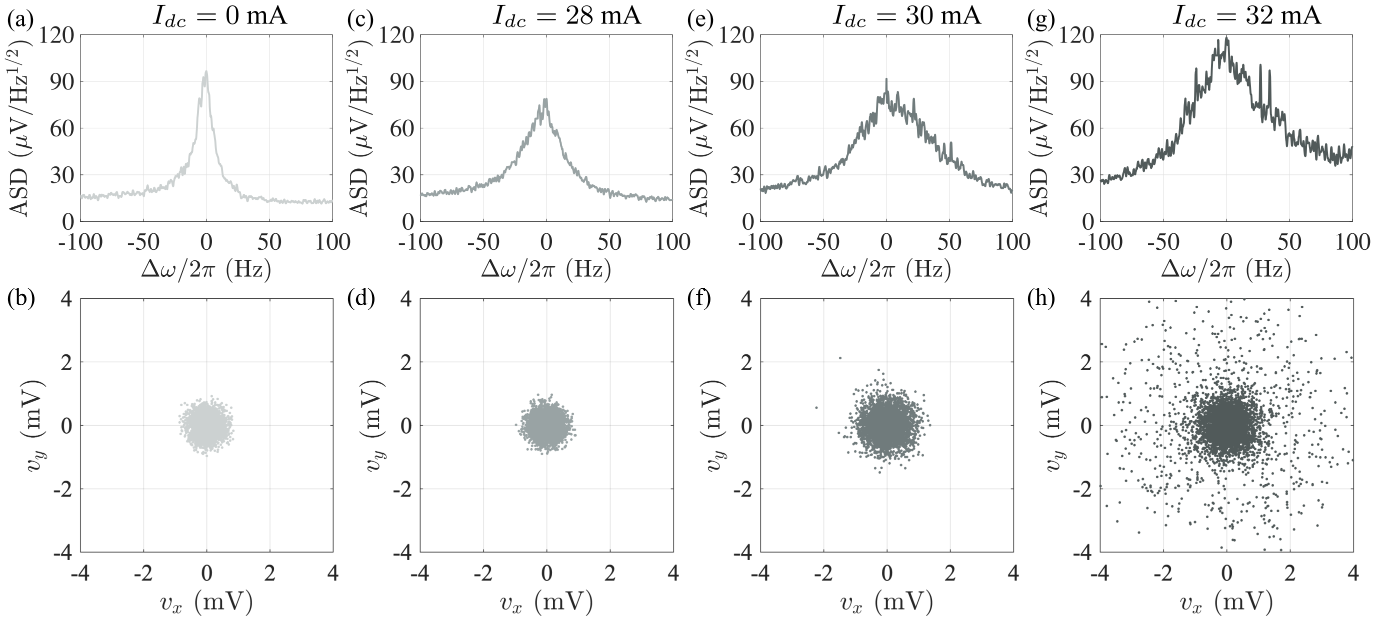

Fig. 7. The (a, c, e, g) amplitude spectral density (ASD) of the thermomechanical noise spectrum for the $L = 50$ μm device as function of frequency detuning $\Delta\omega = \omega - \omega_0$ away from resonance, and the (b, d, f, h) corresponding demodulated noise at resonance, for increasing direct current I_{dc}. v_x and v_y correspond to the two voltage quadratures of the noise, as measured using a lock-in amplifier. The harmonic drive is shut off for these measurements.

we perform additional measurements of the resonance frequency and quality factor of the long-beam device for chamber temperatures varying from -20°C to 70°C, as presented in Fig. 4. The chamber temperature is increased in steps from -20°C to 70°C, and the device is given thirty minutes to thermally equilibrate at each chamber temperature before performing the measurements over I_{dc}. The device Q at low currents decreases monotonically with increasing device temperature, providing a clear indication that this device is TED-limited. Increasing the chamber temperature shifts the temperature hysteresis regime to lower direct currents, as both the resonance frequency and quality factor measurements reveal. For all chamber temperatures, the quality factor plateaus to the same constant level. The plateauing in the quality factor appears to be a thermal phenomenon, but its exact origins remain unclear. The simulations in Fig. 2 suggest that thermal-piezoresistive pumping only influences the quality factor at large currents, beyond the thermal transition region. Neither the temperature-dependent Q_{TED} or Q_{TPP} simulations predict the observed plateauing in Q_{eff}. Thermoelastic dissipation likely saturates at the high device temperatures, but it is difficult to prove this with the present measurements.

The steep drop in resonance frequency at the thermal transition region results from a change in the mechanical stiffness of the resonator, as opposed to a change in the electrostatic softening. To confirm this, we measure the resonance frequency and quality factor as a function of device bias voltage for the $L = 50$ μm and $L = 20$ μm devices. Figure 5(a) plots Q_{eff} and the change in resonance frequency for bias voltages varying from $V_b = 20$ V to $V_b = 60$ V. Increasing the bias voltage increases the slope of the drop in resonance frequency above the thermal transition region, but has very little impact on the current at which the resonance frequency starts to abruptly decrease. Separate FE simulations suggest that at large currents, the proof mass shifts towards one of the side electrodes, increasing the corresponding electrostatic softening. Fig. 5(a) suggests that electrostatic softening plays a role in the long-beam device resonance frequency, but only for currents beyond the thermal transition. The measurements of the short-beam device in Fig. 5(b) seem to suggest that electrostatics play a minimal role in the device behavior. The negligible impact of electrostatics in Fig. 5(b) can be explained by the increased mechanical stiffness in the $L = 20$ μm device compared to the $L = 50$ μm device. For both devices, the bias voltage voltage has a negligible impact on the thermal transition current and the quality factor. This provides additional evidence that the Q_{eff} results from a thermal effect, as opposed to another source such as electrical damping [53], [54]. Below $V_b = 40$ V, the short-beam resonator has too poor of a capacitive readout signal to establish a PLL and perform ringdown measurements.

To provide additional support for the conclusion that the resonance frequency and quality factor behavior result mainly from thermal effects instead of current effects, we performed ringdowns on the long-beam device except after shutting the direct current off for pre-defined intervals, as shown in Fig. 6. At each direct current value, the PLL establishes lock on the resonator, and the direct current is shut off while keeping the harmonic drive on and maintaining lock. After the pause, the harmonic drive is shut off and the ringdown envelope is measured to extract $\omega_0/2\pi$ and Q_{eff}. We repeat the entire current sweep up to 40 mA for pause times of 0 seconds, then 1 second, and finally 2 seconds. At each direct current value, the resonance frequency in Fig. 6(a) increases very abruptly to near its thermal equilibrium value after shutting off the direct current ($\ll$1 ms timescale) followed by a more gradual increase ($\approx$1 s timescale). The quality factor in Fig. 6(b) increases at a slower timescale than the initial drop in resonance frequency. These experiments suggest that the device temperature decreases non-uniformly after shutting off the direct current: the fast actuator/support beam timescale and the slow timescale for the anchors and chip. The resonance frequency is determined by the stiffness in the actuator/support beams and thus the beam temperatures, therefore following their $\approx$10 μs thermal timescale [38]. The resonator quality factor is determined more broadly by the phonon scattering between the mode of interest and the thermal bath, and thus follows the slower timescale of the anchors and the entire floated chip.

We finally consider the noise dynamics of the thermal-piezoresistive resonator in the vicinity of the thermal transition region. We turn off the harmonic drive, and monitor the thermomechanical vibrations directly using a low noise capacitive sensing scheme [55]. A spectrum analyzer is used to measure the scalar spectrum in the vicinity of the resonance frequency, and the noise is simultaneously demodulated at resonance with a lock-in amplifier to extract the two voltage quadratures at a given direct current. Fig. 7 summarizes these measurements for the long-beam device. At $I_{dc} = 0$ mA, the system is in thermal equilibrium, and the demodulated noise consists of the Gaussian noise contributions from the thermomechanical vibrations of the mode and the amplifier Johnson noise. At moderate current, the resonance linewidth increases as Q_{eff} decreases. When the direct current is increased beyond the thermal transition region, the thermomechanical noise spectrum near resonance increases while maintaining the same broad linewidth, and the variance in the thermomechanical noise cloud grows dramatically. The substantial increase in demodulated thermomechanical noise near resonance beyond the thermal transition region could result from a steep increase in the device temperature and corresponding thermomechanical noise force.

III. Conclusion and Future Work

These experiments and simulations reveal the limiting thermal behavior that can impact thermal-piezoresistive cooling in the large current regime: a steep reduction in resonance frequency, an abrupt plateauing in the effective quality factor, and a large increase in thermomechanical fluctuations. Additional experiments and simulations are required to fully understand the highly nonlinear behavior in the thermal transition region. However, our work highlights the importance of chip-scale boundary conditions and their impact on device performance. Thermal-piezoresistive cooling is one application that would benefit from third-order and higher temperature coefficients of elasticity in doped silicon [52], [56]. The experiments reported here could be repeated in non-encapsulated devices, and the mechanical vibrations and microscale heat transport can be imaged at large currents using laser Doppler vibrometry and time-domain thermoreflectance, respectively [57], [58]. Large current experiments could be interesting in nanowire-based thermal-piezoresistive resonators [33], [34]. The behavior of silicon beams at large currents and high temperatures has additional practical implications in micro-tether design for improving inertial sensor fabrication yields [59].

Acknowledgment

The author James M. L. Miller is grateful to Tanya Liu, Farid Soroush, and Woosung Park for assisting with the thermal infrared camera and software. The authors are grateful for the helpful suggestions provided by the anonymous reviewers. The data that support the findings of this study are available from the corresponding authors upon reasonable request.

References

[1] G. Binnig, C. F. Quate, and C. Gerber, "Atomic force microscope," *Phys. Rev. Lett.*, vol. 56, no. 9, p. 930, Mar. 1986.

[2] R. Bogue, "MEMS sensors: Past, present and future," *Sensor Rev.*, vol. 27, no. 1, pp. 7–13, Jan. 2007.

[3] S. Zaliasl *et al.*, "A 3 ppm 1.5×0.8 mm^2 1.0 μA 32.768 kHz MEMS-based oscillator," *IEEE J. Solid-State Circuits*, vol. 50, no. 1, pp. 291–302, Jan. 2015.

[4] R. Ruby, "Review and comparison of bulk acoustic wave FBAR, SMR technology," in *Proc. IEEE Ultrason. Symp.*, Oct. 2007, pp. 1029–1040.

[5] A. Ayari *et al.*, "Self-oscillations in field emission nanowire mechanical resonators: A nanometric DC-AC conversion," *Nano Lett.*, vol. 7, no. 8, pp. 2252–2257, Aug. 2007.

[6] M. Serra-Garcia, A. Foehr, M. Molerón, J. Lydon, C. Chong, and C. Daraio, "Mechanical autonomous stochastic heat engine," *Phys. Rev. Lett.*, vol. 117, no. 1, Jun. 2016, Art. no. 010602.

[7] A. Ganesan, C. Do, and A. Seshia, "Phononic frequency comb via intrinsic three-wave mixing," *Phys. Rev. Lett.*, vol. 118, no. 3, Jan. 2017, Art. no. 033903.

[8] A. W. Hauser, S. Sundaram, and R. C. Hayward, "Photothermocapillary oscillators," *Phys. Rev. Lett.*, vol. 121, no. 15, Oct. 2018, Art. no. 158001.

[9] Z. Liu, X. Yan, M. Qi, Y. Zhu, X. Zhang, and L. Lin, "Asymmetric charge transfer phenomenon and its mechanism in self-excited electrostatic actuator," in *Proc. IEEE Micro Electro Mech. Syst. (MEMS)*, Northern Ireland, U.K., Jan. 2018, pp. 588–591.

[10] C. Urgell *et al.*, "Cooling and self-oscillation in a nanotube electromechanical resonator," *Nature Phys.*, vol. 16, no. 1, pp. 32–37, Jan. 2020.

[11] D. A. Kassie, I. B. Flader, S. Shmulevich, H.-K. Kwon, T. W. Kenny, and D. Elata, "An epi-seal encapsulated Franklin oscillator sustaining more than 200,000,000 electric switching cycles," in *Proc. IEEE 33rd Int. Conf. Micro Electro Mech. Syst. (MEMS)*, Vancouver, BC, Canada, Jan. 2020, pp. 230–233.

[12] S. Houri, D. Hatanaka, M. Asano, and H. Yamaguchi, "Demonstration of multiple internal resonances in a microelectromechanical self-sustained oscillator," *Phys. Rev. A, Gen. Phys.*, vol. 13, no. 1, Jan. 2020, Art. no. 014049.

[13] T. R. Albrecht, P. Grütter, D. Horne, and D. Rugar, "Frequency modulation detection using high-Q cantilevers for enhanced force microscope sensitivity," *J. Appl. Phys.*, vol. 69, no. 2, pp. 668–673, Jan. 1991.

[14] J. Mertz, O. Marti, and J. Mlynek, "Regulation of a microcantilever response by force feedback," *Appl. Phys. Lett.*, vol. 62, no. 19, pp. 2344–2346, May 1993.

[15] P. H. Kim, B. D. Hauer, T. J. Clark, F. Fani Sani, M. R. Freeman, and J. P. Davis, "Magnetic actuation and feedback cooling of a cavity optomechanical torque sensor," *Nature Commun.*, vol. 8, no. 1, pp. 1–6, Dec. 2017.

[16] J. M. L. Miller *et al.*, "Effective quality factor tuning mechanisms in micromechanical resonators," *Appl. Phys. Rev.*, vol. 5, no. 4, Dec. 2018, Art. no. 041307.

[17] P. G. Steeneken *et al.*, "Piezoresistive heat engine and refrigerator," *Nature Phys.*, vol. 7, p. 354, Jan. 2011.

[18] A. Rahafrooz and S. Pourkamali, "Thermal-piezoresistive energy pumps in micromechanical resonant structures," *IEEE Trans. Electron Devices*, vol. 59, no. 12, pp. 3587–3593, Dec. 2012.

[19] J. M. L. Miller *et al.*, "Thermal-piezoresistive tuning of the effective quality factor of a micromechanical resonator," *Phys. Rev. A, Gen. Phys.*, vol. 10, no. 4, Oct. 2018, Art. no. 044055.

[20] A. Hajjam, J. C. Wilson, A. Rahafrooz, and S. Pourkamali, "Self-sustained micromechanical resonant particulate microbalance/counters," in *Proc. IEEE 24th Int. Conf. Micro Electro Mech. Syst.*, Jan. 2011, pp. 629–632.

[21] K.-H. Li, C.-C. Chen, M.-H. Li, and S.-S. Li, "A self-sustained nanomechanical thermal-piezoresistive oscillator with ultra-low power consumption," in *IEDM Tech. Dig.*, San Francisco, CA, USA, Dec. 2014, pp. 2–22.

[22] G. Lehee, R. Anciant, F. Souchon, A. Berthelot, P. Rey, and G. Jourdan, "P-type silicon nanogauge based self-sustained oscillator," in *Proc. 19th Int. Conf. Solid-State Sensors, Actuat. Microsyst. (TRANSDUCERS)*, Kaohsiung, Taiwan, Jun. 2017, pp. 444–447.

[23] C.-C. Chu, S. Dey, T.-Y. Liu, C.-C. Chen, and S.-S. Li, "Thermal-piezoresistive SOI-MEMS oscillators based on a fully differential mechanically coupled resonator array for mass sensing applications," *J. Microelectromech. Syst.*, vol. 27, no. 1, pp. 59–72, Feb. 2018.

[24] H. Zhu, C. Tu, J. E.-Y. Lee, and L. Rufer, "Active electronic cancellation of nonlinearity in a high-Q longitudinal-mode silicon resonator by current biasing," in *Proc. Eur. Freq. Time Forum (EFTF)*, Neuchatel, Switzerland, Jun. 2014, pp. 12–15.

[25] E. Mehdizadeh, V. Kumar, and S. Pourkamali, "Sensitivity enhancement of Lorentz force MEMS resonant magnetometers via internal thermal-piezoresistive amplification," *IEEE Electron Device Lett.*, vol. 35, no. 2, pp. 268–270, Feb. 2014.

[26] X. Guo, E. Mehdizadeh, V. Kumar, A. Ramezany, and S. Pourkamali, "An ultra high-Q micromechanical in-plane tuning fork," in *Proc. IEEE Sensors*, Valencia, Spain, Nov. 2014, pp. 990–993.

[27] A. Ramezany, M. Mahdavi, and S. Pourkamali, "Nanoelectromechanical resonant narrow-band amplifiers," *Microsystems Nanoengineering*, vol. 2, no. 1, p. 16004, Dec. 2016. [Online]. Available: http://www.nature.com/articles/micronano20164

[28] A. Ramezany, S. Babu, V. Kumar, J.-B. Lee, and S. Pourkamali, "Resonant piezoresistive amplifiers: Towards single element nano-mechanical RF front ends," in *Proc. IEEE 30th Int. Conf. Micro Electro Mech. Syst. (MEMS)*, Las Vegas, NV, USA, Jan. 2017, pp. 72–75.

[29] H. J. Hall *et al.*, "Mode selection behavior of VHF thermal-piezoresistive self-sustained oscillators," in *Proc. 17th Int. Conf. Solid-State Sensors, Actuat. Microsyst. (TRANSDUCERS EUROSENSORS XXVII)*, Barcelona, Spain, Jun. 2013, pp. 1392–1395.

[30] A. Ramezany and S. Pourkamali, "Ultrahigh frequency nanomechanical piezoresistive amplifiers for direct channel-selective receiver front-ends," *Nano Lett.*, vol. 18, no. 4, pp. 2551–2556, Apr. 2018.

[31] P. Janioud *et al.*, "Thermal piezoresistive back action enhancement using an innovative design of silicon nanobeam," in *Proc. IEEE 32nd Int. Conf. Micro Electro Mech. Syst. (MEMS)*, Seoul, South Korea, Jan. 2019, pp. 157–160.

[32] A. A. Zope, J.-H. Chang, T.-Y. Liu, and S.-S. Li, "A CMOS-MEMS thermal-piezoresistive oscillator for mass sensing applications," *IEEE Trans. Electron Devices*, vol. 67, no. 3, pp. 1183–1191, Mar. 2020.

[33] P. Janioud *et al.*, "Switching thermal piezoresistive oscillators from damped to self-sustained regime using tunable resistors," in *Proc. 20th Int. Conf. Solid-State Sensors, Actuat. Microsyst. (TRANSDUCERS EUROSENSORS)*, Berlin, Germany, Jun. 2019, pp. 2162–2165.

[34] G. Lehee, F. Souchon, J.-C. Riou, A. Bosseboeuf, and G. Jourdan, "Low power damping control of a resonant sensor using back action in silicon nanowires," in *Proc. IEEE 29th Int. Conf. Micro Electro Mech. Syst. (MEMS)*, Shanghai, China, Jan. 2016, pp. 99–102.

[35] D. B. Heinz, V. A. Hong, C. H. Ahn, E. J. Ng, Y. Yang, and T. W. Kenny, "Experimental investigation into stiction forces and dynamic mechanical anti-stiction solutions in ultra-clean encapsulated MEMS devices," *J. Microelectromech. Syst.*, vol. 25, no. 3, pp. 469–478, Jun. 2016.

[36] D. D. Shin, C. H. Ahn, Y. Chen, D. L. Christensen, I. B. Flader, and T. W. Kenny, "Environmentally robust differential resonant accelerometer in a wafer-scale encapsulation process," in *Proc. IEEE 30th Int. Conf. Micro Electro Mech. Syst. (MEMS)*, Las Vegas, NV, USA, Jan. 2017, pp. 17–20.

[37] S. Sundaram, "Thermally-actuated piezoresistively-sensed mechanical silicon oscillator," M.S. thesis, Massachusetts Inst. Technol., Cambridge, MA, USA, 2014.

[38] S. Sundaram and D. Weinstein, "Bulk mode piezoresistive thermal oscillators: Time constants and scaling," *IEEE Trans. Ultrason., Ferroelectr., Freq. Control*, vol. 62, no. 8, pp. 1554–1562, Aug. 2015.

[39] A. Cywar, G. Bakan, C. Boztug, H. Silva, and A. Gokirmak, "Phase-change oscillations in silicon microwires," *Appl. Phys. Lett.*, vol. 94, no. 7, Feb. 2009, Art. no. 072111.

[40] A. Cywar *et al.*, "Scaling of silicon phase-change oscillators," *IEEE Electron Device Lett.*, vol. 32, no. 11, pp. 1486–1488, Nov. 2011.

[41] N. Ono, K. Kitamura, K. Nakajima, and Y. Shimanuki, "Measurement of Young's modulus of silicon single crystal at high temperature and its dependency on boron concentration using the flexural vibration method," *Jpn. J. Appl. Phys.*, vol. 39, no. 2R, p. 368, 2000.

[42] P. Kury and M. Horn-von Hoegen, "Impact of thermal dependence of elastic constants on surface stress measurements," *Rev. Sci. Instrum.*, vol. 75, no. 5, pp. 1357–1358, May 2004.

[43] A. Masolin, P.-O. Bouchard, R. Martini, and M. Bernacki, "Thermo-mechanical and fracture properties in single-crystal silicon," *J. Mater. Sci.*, vol. 48, no. 3, pp. 979–988, Feb. 2013.

[44] H. R. Shanks, P. D. Maycock, P. H. Sidles, and G. C. Danielson, "Thermal conductivity of silicon from 300 to 1400 K," *Phys. Rev.*, vol. 130, no. 5, p. 1743, Jun. 1963.

[45] N. D. Arora, J. R. Hauser, and D. J. Roulston, "Electron and hole mobilities in silicon as a function of concentration and temperature," *IEEE Trans. Electron Devices*, vol. 29, no. 2, pp. 292–295, Feb. 1982.

[46] R. N. Candler *et al.*, "Single wafer encapsulation of MEMS devices," *IEEE Trans. Adv. Packag.*, vol. 26, no. 3, pp. 227–232, Aug. 2003.

[47] Y. Yang, E. J. Ng, Y. Chen, I. B. Flader, and T. W. Kenny, "A unified epi-seal process for fabrication of high-stability microelectromechanical devices," *J. Microelectromech. Syst.*, vol. 25, no. 3, pp. 489–497, Jun. 2016.

[48] Y. Kanda, "A graphical representation of the piezoresistance coefficients in silicon," *IEEE Trans. Electron Devices*, vol. 29, no. 1, pp. 64–70, Jan. 1982.

[49] J. Rodriguez, *et al.*, "Direct detection of anchor damping in MEMS tuning fork resonators," *J. Microelectromech. Syst.*, vol. 27, no. 5, pp. 800–809, 2018.

[50] P. M. Polunin, Y. Yang, M. I. Dykman, T. W. Kenny, and S. W. Shaw, "Characterization of MEMS resonator nonlinearities using the ringdown response," *J. Microelectromech. Syst.*, vol. 25, no. 2, pp. 297–303, Apr. 2016.

[51] C. J. Glassbrenner and G. A. Slack, "Thermal conductivity of silicon and germanium from 3°K to the melting point," *Phys. Rev.*, vol. 134, no. 4A, pp. A1058–A1069, May 1964.

[52] E. J. Ng, V. A. Hong, Y. Yang, C. H. Ahn, C. L. M. Everhart, and T. W. Kenny, "Temperature dependence of the elastic constants of doped silicon," *J. Microelectromech. Syst.*, vol. 24, no. 3, pp. 730–741, Jun. 2015.

[53] J. Rieger, T. Faust, M. J. Seitner, J. P. Kotthaus, and E. M. Weig, "Frequency and Q factor control of nanomechanical resonators," *Appl. Phys. Lett.*, vol. 101, no. 10, Sep. 2012, Art. no. 103110.

[54] N. E. Bousse, J. M. L. Miller, H.-K. Kwon, G. D. Vukasin, and T. W. Kenny, "Quality factor tuning of micromechanical resonators via electrical dissipation," *Appl. Phys. Lett.*, vol. 116, no. 2, Jan. 2020, Art. no. 023506.

[55] J. M. L. Miller *et al.*, "Thermomechanical-noise-limited capacitive transduction of encapsulated MEM resonators," *J. Microelectromech. Syst.*, vol. 28, no. 6, pp. 965–976, Dec. 2019.

[56] A. Jaakkola, M. Prunnila, T. Pensala, J. Dekker, and P. Pekko, "Determination of doping and temperature-dependent elastic constants of degenerately doped silicon from MEMS resonators," *IEEE Trans. Ultrason., Ferroelectr., Freq. Control*, vol. 61, no. 7, pp. 1063–1074, Jul. 2014.

[57] L. L. Li, E. L. Holthoff, L. A. Shaw, C. B. Burgner, and K. L. Turner, "Noise squeezing controlled parametric bifurcation tracking of MIP-coated microbeam MEMS sensor for TNT explosive gas sensing," *J. Microelectromech. Syst.*, vol. 23, no. 5, pp. 1228–1236, Oct. 2014.

[58] A. Sood *et al.*, "Quasi-ballistic thermal transport across MoS_2 thin films," *Nano Lett.*, vol. 19, no. 4, pp. 2434–2442, Apr. 2019.

[59] I. B. Flader *et al.*, "Micro-tethering for fabrication of encapsulated inertial sensors with high sensitivity," *J. Microelectromech. Syst.*, vol. 28, no. 3, pp. 372–381, Jun. 2019.

James M. L. Miller received the B.S. degree in mechanical engineering from Michigan State University in 2014, and the M.S. degree in mechanical engineering from Stanford University in 2016, where he is currently pursuing the Ph.D. degree with support from the National Defense Science and Engineering (NDSEG) Fellowship and the E. K. Potter Stanford Graduate Fellowship. His research interests include nonlinearities, fluctuations, and dissipation tuning mechanisms in MEM resonators for sensors and oscillators.

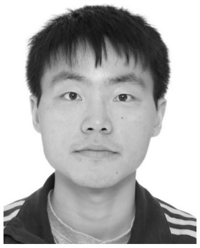

Haoshen Zhu (Member, IEEE) received the B.E. degree in electrical engineering from the Wuhan University of Technology, Wuhan, China, in 2009, and the Ph.D. degree in electronics engineering from the City University of Hong Kong, Hong Kong, in 2015. He is currently an Associate Professor with the School of Electronics and Information Engineering, South China University of Technology. His research interests include modeling, fabrication of MEMS resonators, as well as RF MEMS filters and their applications for timing and frequency control.

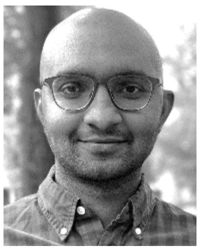

Subramanian Sundaram received the B.E. (Hons.) degrees in electrical engineering and mechanical engineering from the Birla Institute of Technology and Science (BITS), Pilani, India, in 2010, and the S.M. and Ph.D. degrees in electrical engineering and computer science from the Massachusetts Institute of Technology (MIT), Cambridge, MA, USA, in 2014 and 2018, respectively. He is currently an American Heart Association Postdoctoral Fellow at Boston University and the Wyss Institute for Biologically Inspired Engineering, Harvard University. His research interests include robotics, advanced fabrication, and tissue engineering.

Gabrielle D. Vukasin received the B.A. degree in astrophysics and mathematics from Williams College in 2014, and the M.S. degree in mechanical engineering from Tufts University in 2016. She is currently pursuing the Ph.D. degree in mechanical engineering with Stanford University. Her research interests include the design and fabrication of MEM resonators with a focus on the characterization of energy loss mechanisms using wide-range temperature measurements of the quality factor.

Yunhan Chen received the B.S. degree in mechanical engineering from Tsinghua University, Beijing, China, in 2011, and the M.S. and Ph.D. degrees in mechanical engineering from Stanford University, Stanford, CA, USA, in 2013 and 2017, respectively. During his studies, he was supported by the Stanford Graduate Fellowship. His research interests include microfabrication technologies, ovenized MEMS resonators, and MEMS inertial sensors.

Ian B. Flader received the B.S. degree *(summa cum laude)* in mechanical engineering from The University of Tennessee, Knoxville, TN, USA, in 2012, and the M.S. and Ph.D. degrees in mechanical engineering from Stanford University, in 2016 and 2018, respectively. His research interests include disk resonating gyroscopes, resonant accelerometers, encapsulated inertial sensors, modal coupling, novel MEMS fabrication techniques, topological and gradient-free optimization, and automatic control.

Dongsuk D. Shin received the B.S. degree in mechanical engineering from Johns Hopkins University, Baltimore, MD, USA, in 2014, and the M.S. and Ph.D. degrees from Stanford University, Stanford, CA, USA, in 2019, where he was supported by the Stanford Graduate Fellowship. His research interests include design, fabrication, and characterization of MEMS inertial sensors, including resonant accelerometers and disk resonating gyroscopes.

Thomas W. Kenny (Senior Member, IEEE) received the B.S. degree from the University of Minnesota in 1983, and the M.S. and Ph.D. degrees from the University of California at Berkeley, in 1987 and 1989, respectively, all in physics. From 1989 to 1993, he was at JPL/NASA, Pasadena, CA, USA, where his research focused on the development of electron-tunneling high-resolution microsensors. In 1994, he joined the Department of Mechanical Engineering, Stanford University, Stanford, CA, USA, where he directs microsensor-based research in a variety of areas, including resonators, wafer-scale packaging, cantilever beam force sensors, microfluidics, and novel fabrication techniques for micromechanical structures. He was the Founder and CTO of Cooligy (now a division of Emerson), a microfluidics chip cooling component manufacturer, and was the Founder and Board Member of SiTime Corporation (now a division of MegaChips), the developer of timing references using MEM resonators. He is the Founder and Board Member of Applaud Medical, developing noninvasive therapies for kidney stones. From 2006 to 2010, he served as the Program Manager of the Microsystems Technology Office at DARPA, starting and managing programs in thermal management, nanomanufacturing, manipulation of Casimir forces, and the Young Faculty Award. He is currently the Richard Weiland Professor of Mechanical Engineering and the Senior Associate Dean of Engineering for Student Affairs. He has authored or coauthored over 250 scientific papers and holds 50 issued patents, and has been an Advisor for over 50 graduated Ph.D. students from Stanford University. He was the General Chairman of the 2006 Hilton Head Solid-State Sensors, Actuators, and Microsystems Workshop, and the General Chair of the Transducers 2015 meeting in Anchorage.